Chemical Geology 681 (2025) 122712

Contents lists available at ScienceDirect

Chemical Geology

journal homepage: www.elsevier.com/locate/chemgeo

Twice the global average carbon burial efficiency in the Helgoland Mud Area of the North Sea: Insights into carbon sequestration in small-size depocenters on sand-dominated shelves

Bingbing Wei [a,b,*], Daniel Müller [a,e], Stephanie Kusch [c], Lu Niu [a], Jens Hefter [a], Lasse Sander [d], Ulrike Hanz [a], Gesine Mollenhauer [a,b,e], Guodong Jia [f,g], Sabine Kasten [a,b,e], Moritz Holtappels [a,b]

[a] Alfred Wegener Institute Helmholtz Centre for Polar and Marine Research, Bremerhaven, Germany
[b] MARUM - Center for Marine Environmental Sciences, University of Bremen, Bremen, Germany
[c] ISMER - Institute of Marine Sciences, University of Quebec Rimouski, Rimouski, Canada
[d] Alfred Wegener Institute Helmholtz Centre for Polar and Marine Research, List/Sylt, Germany
[e] Faculty of Geosciences, University of Bremen, Bremen, Germany
[f] State Key Laboratory of Marine Geology, Tongji University, Shanghai, China
[g] Southern Marine Science and Engineering Guangdong Laboratory (Zhuhai), Zhuhai, China

ARTICLE INFO

Editor: Christian France-Lanord

Keywords:
Sand-dominated shelves
Small-size depocenters
Organic carbon burial
Helgoland Mud Area (HMA)
Stable carbon isotope
Fatty acids and alkanes

ABSTRACT

Continental shelves are integral to the global carbon cycle, yet uncertainties persist about the nature and extent of carbon burial, particularly in sand-dominated areas. In the sand-dominated North Sea, the Helgoland Mud Area (HMA) emerges as a small-size mud depocenter, surrounded by sandy sediments that do not accumulate organic carbon (OC) and are separated from adjacent rivers. Such small-size depocenters, common on high-energy shelves, have underexplored OC degradation and burial efficiencies due to their limited individual size. Since sandy sediments with interspersed small-size depocenter cover ~50 % of global shelves, these depocenters may collectively offer greater OC burial capacity than previously recognized.

This study investigated the composition, degradation, and sequestration of OC from terrestrial (OC_{terr}) and marine (OC_{mar}) sources in surface sediments of the HMA and adjacent sandy areas using bulk (mean grain size, OC content, loading and ^{13}C isotope composition) and molecular (fatty acids and alkanes) analyses. Our results, derived from a two end-member mixing model based on $\delta^{13}C$ values of bulk OC, revealed that OC_{terr} dominates (~74 %) the sedimentary OC in both areas, with OC_{mar} contributing ~26 %. The HMA exhibited OC_{terr} and OC_{mar} contents ~5 times higher than in the sandy areas. Both OC_{terr} and OC_{mar} loadings negatively correlated with mean grain size, indicating reduced OC degradation in muddy sediments. Molecular analysis further revealed that OC_{terr} in the HMA is less refractory compared to adjacent sandy regions. These differences are attributed to differences in porewater transport, oxygen penetration depths and exposure times, all of which influence OC preservation, despite the important role of mineral protection. OC_{terr} and OC_{mar} accumulation fluxes in the HMA were calculated at $(6.75 \pm 0.61) \times 10^{-3}$ and $(2.54 \pm 0.68) \times 10^{-3}$ Tg C/yr, respectively, representing 34.3 % of OC_{terr} export from adjacent rivers and 2.8 % of net OC_{mar} production in the HMA. These values are twice the global average for shelf areas, highlighting the exceptional efficiency of the HMA as a carbon sink and hinting at the significance of small-size depocenters within sandy areas in the global carbon cycle.

1. Introduction

Continental shelves occupy only 7–10 % of the global seafloor but are an important component of the global carbon cycle and budget. They contribute up to 30 % of marine primary production, 30–50 % of inorganic carbon, and about 80 % of organic carbon (OC) burial in marine sediments (Bauer et al., 2013). However, considerable uncertainty remains about the nature and magnitude of carbon burial as continental shelves are inherently dynamic and spatially heterogeneous systems (Bianchi et al., 2018). This is most clearly reflected in the

* Corresponding author at: Alfred Wegener Institute Helmholtz Centre for Polar and Marine Research, Bremerhaven, Germany.
E-mail address: bingbing.wei@awi.de (B. Wei).

https://doi.org/10.1016/j.chemgeo.2025.122712
Received 27 August 2024; Received in revised form 17 February 2025; Accepted 25 February 2025
Available online 27 February 2025

widespread occurrence of sandy, non-accumulating sediments, despite high overlying primary production (Emery, 1968). In sand-dominated shelf regions, strong tides and waves generate high bottom shear stress that hinders the accumulation of fine-grained, OC-rich particles, enhancing OC mineralization in the water column and driving lateral transport to areas with better sedimentation condition (e.g., de Haas et al., 2002; Crockett and Nittrouer, 2004; Bockelmann et al., 2018). Such condition for OC accumulation may be attributed to greater water depths (resulting in decreased tidal currents), reduced net transport due to specific hydrodynamics, strong terrestrial input, or a combination of these factors (de Haas et al., 2002; Porz et al., 2021). Often small in their individual areal extent, OC depocenters on sandy shelves are easily overlooked, yet they may collectively contribute significantly to global OC burial. Moreover, they provide a natural laboratory for analyzing OC quality and degradation states across transitions from fine to coarser sediments under similar conditions of OC supply. In shallow coastal seas, understanding how heterogenous sedimentation conditions influence the degradation and preservation of OC from different sources is particularly important, as these conditions could change under future climatic scenarios.

Shelf sediments primarily receive OC from marine (OC_{mar}) and terrestrial (OC_{terr}) sources, which includes biospheric OC_{terr} (from photosynthesis) and petrogenic OC_{terr} (from rocks) (Galy et al., 2015). OC_{mar} is generally more reactive than OC_{terr}, leading to higher remineralization rates (Burdige, 2005; Zonneveld et al., 2010). Biospheric OC_{terr} can also be reactive and undergo partial oxidation during transport, thus contributing to CO_2 recycling (Galy et al., 2015; Wei et al., 2021). Only the burial of OC_{mar} and biospheric OC_{terr} that escapes oxidation leads to long-term carbon sequestration, whereas petrogenic OC_{terr} recycling and reburial does not affect atmospheric CO_2 and its oxidation releases CO_2 (Hilton and West, 2020). Therefore, OC source, sedimentation rate, and oxygen exposure time affect atmospheric CO_2 levels over different timescales (Hartnett et al., 1998; Zonneveld et al., 2010; Galy et al., 2015; Hemingway et al., 2019; Hilton and West, 2020).

The North Sea, an epicontinental sea on the northwest European passive continental margin, is characterized by high tides and wave energies, resulting in extensive sandy areas that do not accumulate much OC despite a high primary production ($\sim 90.3 \times 10^{-3}$ Tg C/yr; van Leeuwen et al., 2013). Much of the OC_{mar} is degraded either in the water column (van Beusekom et al., 1999) or in the sandy sediments (Ahmerkamp et al., 2017). The Helgoland Mud Area (HMA), translated from the proper German name "Helgoländer Schlickgebiet", is a small yet significant depocenter within the sand-dominated German Bight of the North Sea, spanning approximately 500 km^2 with shallow waters ranging from 15 to 35 m in depth. Throughout the Holocene it has accumulated considerable amounts of finer-grained sediments (dominated by silt and very fine sand) in contrast to the surrounding sandy area, at a sedimentation rate of several mm/yr (Bockelmann et al., 2018; Diesing et al., 2021; Hebbeln et al., 2003). Therefore, the sediments in the HMA are generally much coarser than in other mud areas in the world such as the Yangtze River-derived Zhe-Min mud area (mean grain size: 16 ± 4 μm; Yu et al., 2024) or the Pearl River-derived mud area (28 ± 16 μm; Wei et al., 2020). The mechanism for the continuous fine-grained sediment deposition in the HMA is under investigation, but it can likely be attributed to the interaction of wind-driven coastal circulation with two frontal systems: a salinity front located in the shoreward part of the HMA and a tidal mixing front in the seaward part of the HMA (Krause et al., 1986; Porz et al., 2021). These fronts effectively deliver fine-grained sediments to the HMA and trap them within the area. The salinity front remains consistently positioned over the HMA, supporting year-round sediment deposition. The HMA provides ideal conditions for studying the degradation and burial efficiency of OC from different sources in a small-size depocenter and along the transition to adjacent sandy areas.

To characterize sediment and OC compositions, we conducted a high-resolution sampling of surface sediments of the HMA and adjacent sandy areas and analyzed sediment grain size, OC and total nitrogen (TN) contents, stable carbon isotope composition of OC ($\delta^{13}C_{OC}$), and abundances of source-specific fatty acids (FAs) and alkanes. This study aims to (1) characterize and quantify the composition and origin of OC in these sediments; (2) assess the degradation and sequestration potentials of OC_{mar} and OC_{terr} using molecular markers; (3) estimate the burial fluxes of OC_{terr} and OC_{mar} in the HMA. The insights gained will enhance our understanding of current carbon cycling in shallow shelf systems under heterogenous sedimentation conditions at the seafloor. Additionally, as part of the project APOC, this work improves the interpretation of the HMA's historical sedimentary record and contributes to evaluating the carbon storage capacity of marine sediments in the North Sea, helping to assess potential preservation measures within the appropriate governance framework. Overall, this study emphasizes the role of small-size OC depocenter that are interspersed in high-energy sand shelves and highlights their potential significance in the global carbon budget.

2. Materials and methods

2.1. Sampling

During a dedicated sampling campaign in the framework of the project APOC with the R/V Heincke (HE-595) in March and April 2022, surface sediments (0–2 cm) were collected from 57 sites in the HMA and surrounding sandy areas (Fig. 1A) using a grab sampler or multiple corer. During the sampling campaign, these samples were collected specifically for the analyses described below, and all analytical procedures were performed on the same set of samples to ensure consistent treatment for robust statistical analysis. Of the 57 sampling sites, 9 locations were identical to those presented by Müller et al. (2024), allowing seamless integration of their results where applicable. A full station list with positions and bulk properties of surface sediments is compiled in Supplementary Table S1. All sediment samples were stored at −20 °C on board and then freeze-dried upon return to the laboratory.

2.2. Grain size measurements

The grain size of sediments was determined with a Cilas 1180 laser-diffraction particle analyzer (range 0.04–2500 μm) and the mean grain size was calculated using the statistical program Gradistat 9.1 (Blott and Pye, 2001). Prior to analysis, carbonate and OC were removed with 30 % acetic acid and 12 % hydrogen peroxide. The surface area (SA) was calculated from the grain size distribution of the sediments according to Mayer and Rossi (1982):

$$SA_{cal}\ (m^2/g) = 67.6\ X_{<2} + 27.4\ X_{2\text{–}3.9} + 19.5\ X_{3.9\text{–}7.8} + 10.6\ X_{7.8\text{–}15.6} + 5.8\ X_{15.6\text{–}31} + 2.8\ X_{31\text{–}44} + 1.9\ X_{44\text{–}62} + 3.1\ X_{>62} \quad (1)$$

$$SA_{cor}\ (m^2/g) = 1.746 \times SA_{cal} - 4.174 \quad (2)$$

where X is the fraction of sediment of the respective size fraction indicated in the subscripts (in μm). Because the dominant contribution to

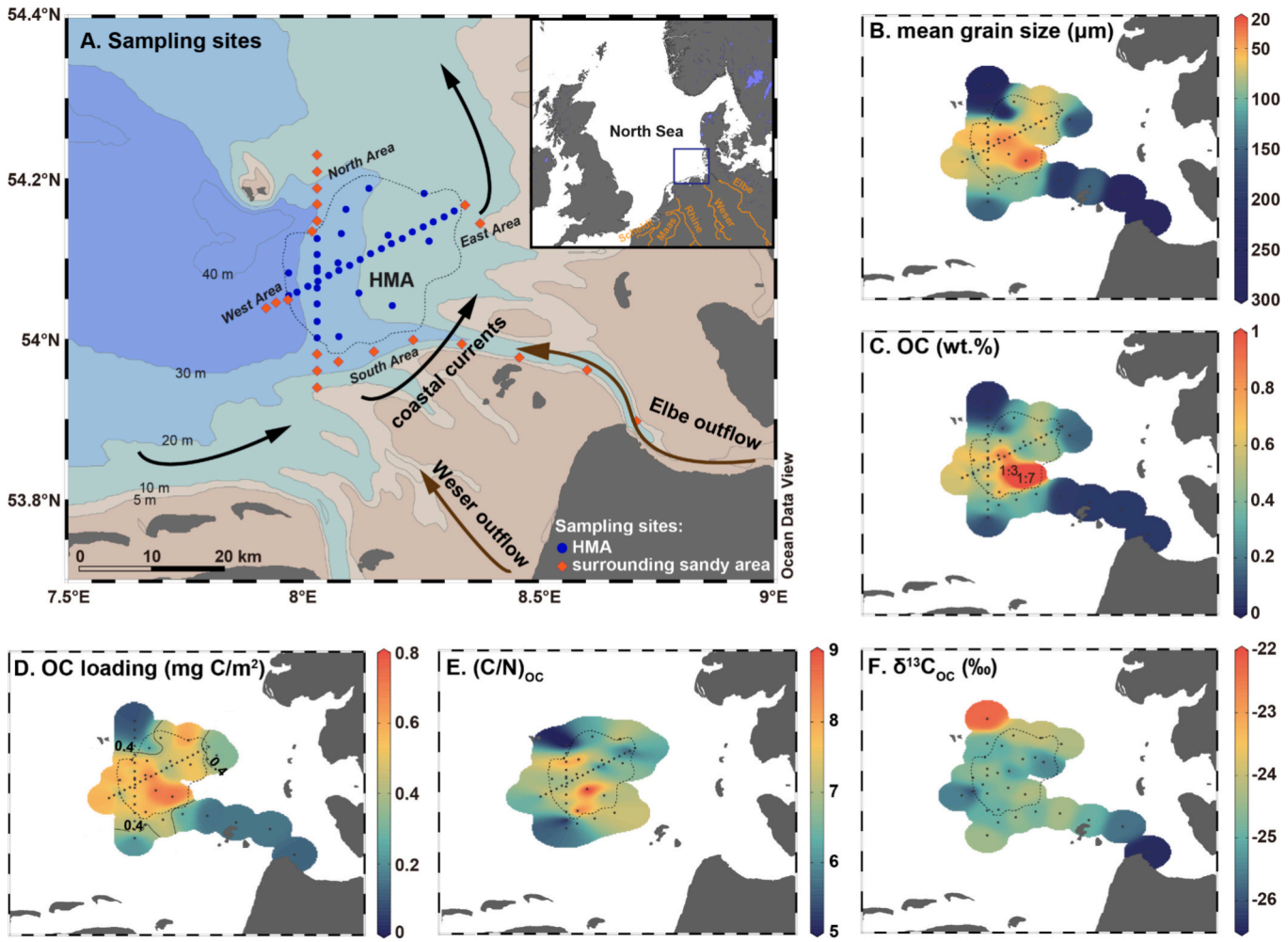

Fig. 1. (A) Sampling locations (coastal currents from de Haas et al. (2002)) and spatial distribution of (B) mean grain size (note reverse scale, $n = 56$), (C) OC content ($n = 57$), (D) OC loading ($n = 54$), (E) $(C/N)_{OC}$ ($n = 45$), and (F) $\delta^{13}C_{OC}$ in the surface sediments of the HMA and surrounding sandy areas ($n = 31$). In panels A to F, the dashed contour separates the HMA from the surrounding sandy areas following von Haugwitz et al. (1988). Maps were generated using the Ocean Data View software (Schlitzer, 2019), stations used for plots B–F are displayed as black dots.

SA_{cal} is related to the mud fraction (<63 µm; silt and clay), only samples with a minimum mud content of 5 % were considered. SA_{cal} was further corrected using the established relationship between measured and calculated SA (Eq. (2); Sun et al., 2024) to better align with the measured SA. The measured OC content was divided by the SA_{cor} to calculate the OC loadings.

2.3. Elemental and stable carbon isotopic analysis

To analyze the OC content of surface sediments, about 0.1 g of sediments was treated with 0.5 mL of 6 M HCl in a crucible and heated on a hot plate at 60 °C overnight to remove carbonates. The OC content of surface sediments was then determined using a carbon-sulfur analyzer (CS-125, Leco). A sediment reference standard was analyzed every 11 runs to monitor average absolute deviation from known OC content. The OC content of surface sediments was then corrected for this deviation, with an accuracy of ≤0.01 wt%. The total carbon (TC) and nitrogen (TN) contents of the samples were analyzed using a carbon-nitrogen-sulfur analyzer (Elemental III, Vario) and used to calculate carbonate contents ($\%CaCO_3 = (\%TC - \%OC) \times 8.333$) and the mass ratio of OC to TON content ($(C/N)_{OC}$), which was corrected for mineral-associated inorganic N according to the method of Schubert and Calvert (2001). The stable carbon isotope composition of OC in surface sediments ($\delta^{13}C_{OC}$) was measured in duplicate using a Thermo Delta isotope ratio mass spectrometer coupled to a Carlo Erba elemental analyzer. During measurements, a reference standard was analyzed every 12 runs to monitor average absolute deviation from the known $\delta^{13}C$ value. The $\delta^{13}C_{OC}$ values of surface sediments was then corrected for this deviation. $\delta^{13}C_{OC}$ values are given in per mil notation relative to the Vienna Pee Dee Belemnite standard. The standard deviation of duplicate analyses ranged from 0.01 ‰ to 0.18 ‰, with an average of 0.10 ‰.

2.4. Lipid extraction and separation

The methods used for extraction and isolation of fatty acids (FA) and alkanes are similar to those described by Mollenhauer and Eglinton (2007) and Wei et al. (2021). Approximately 5–10 g of sediment from the HMA and 20–30 g of sediment from the sandy area were extracted 4 times by ultrasonication with dichloromethane: methanol (9:1, *v/v*) for 15 min. For quantification of FAs and alkanes, known amounts of 19-methylarachidic acid and squalane were added as internal standards prior to extraction. Supernatants from each extraction were obtained by centrifugation and combined. The total lipid extracts were concentrated to ~1 mL by rotary evaporation and transferred to 4 mL vials. After evaporation under a nitrogen stream, the total lipid extracts were saponified for 2 h at 80 °C with 1 mL of KOH (0.1 M) in methanol: H_2O (9:1, *v/v*). After saponification, the neutral fractions were liquid-liquid extracted with *n*-hexane and alkanes were eluted from the neutral

fractions by silica gel column chromatography with *n*-hexane. The remaining KOH solution was acidified to pH = 1, from which FA were liquid-liquid extracted into dichloromethane. The extracted and dried FAs were converted to methyl ester derivatives (FAMEs) in methanol: HCl (95:5, v/v) at 60 °C for 12 h. After methylation, the FAME fraction was further purified by silica gel column chromatography using dichloromethane: hexane (2:1, *v/v*) to remove residual polar compounds.

FAMEs and alkanes were analyzed on a 7890 A gas chromatograph (GC) equipped with a DB-5MS fused silica capillary column (60 m, 250 μm, 0.25 μm) and a flame ionization detector (FID). Helium was used as the carrier gas (1.5 mL/min), and the GC oven was heated using the following temperature program: 60 °C for 1 min, 20 °C/min to 150 °C, 6 °C/min to 320 °C, and a final hold time of 35 min. Peak areas were determined by integrating the respective peaks and concentrations were calculated against the internal standards. FAME contents were subsequently corrected for the derivative methyl carbon to determine FA contents. FAs and alkanes were normalized to OC content.

2.5. Source apportionment calculation

A two end-member mixing model based on the $\delta^{13}C_{OC}$ values was used to quantify the relative fractional contributions of OC_{terr} (f_{terr}) and OC_{mar} (f_{mar}) in the study area as follows:

$$f_{terr} \times \delta^{13}C_{terr} + f_{mar} \times \delta^{13}C_{mar} = \delta^{13}C_{OC} \quad (3)$$

$$f_{terr} + f_{mar} = 1 \quad (4)$$

where $\delta^{13}C_{OC}$ represents the measured bulk sediment $\delta^{13}C$ value, $\delta^{13}C_{terr}$ and $\delta^{13}C_{mar}$ represent the OC_{terr} and OC_{mar} $\delta^{13}C$ end-member values, respectively, and f_{terr} and f_{mar} represent their corresponding fractional contributions. We use the mean $\delta^{13}C_{OC}$ value of the lower Elbe SPM (−27.2 ± 0.7 ‰; Zander et al., 2020), which contains a mixture of plant detritus, soil- and bedrock-OC, to represent the OC_{terr} end-member. Note that the petrogenic and biospheric OC_{terr} pools in this end-member cannot be distinguished based on their ^{13}C isotope composition. There is no reported $\delta^{13}C_{OC}$ value for Weser SPM, but we assume it is comparable to that of the Elbe River due to the proximity of the river basins and their similar climatic (and ecosystem/vegetation) conditions, as suggested to some extent by a comparable $\delta^{13}C_{OC}$ value (−27.0 ‰; Megens et al., 2001) of SPM in the estuary of the Maas, Rhine, and Scheldt rivers to the southwest of the Elbe and Weser. The Maas, Rhine and Scheldt rivers (total SPM export flux of ~1.52 Mt./yr; Milliman and Farnsworth, 2011) may also supply SPM to the HMA via coastal currents, although the transport distance from this source to the HMA is much greater (~500 km) than from the Elbe and Weser rivers (~60 km). Regardless, given the similarity of the SPM $\delta^{13}C_{OC}$ values, any such contributions will not bias our mass balance results, and thus will not impact the quantification of OC_{terr} contributions. Surface SPM from the North Sea composed almost entirely of algae yielded a $\delta^{13}C_{OC}$ value of −17.8 ‰ (Megens et al., 2001). We use this value to represent the OC_{mar} end-member, with ±1 ‰ uncertainty to account for potential seasonal changes in the $\delta^{13}C_{mar}$ end-member composition (Middelburg and Nieuwenhuize, 1998 and references therein). A Bayesian Markov chain Monte Carlo simulation was used here, and the values of the individual source end-members were assumed to be normally distributed (Andersson et al., 2015). Of the 10^8 random samples, 10^6 were taken from the normal distribution of each end-member within the given mean and standard deviation to simultaneously fulfill the given system in simulations. The mean relative contributions and the standard deviation of OC_{mar} and OC_{terr} were then estimated (Andersson et al., 2015).

2.6. Calculation of sediment and OC accumulation fluxes

Recently, Müller et al. (2024) provided detailed analyses of sedimentation and OC accumulation rates in the HMA using sediment samples from the same expedition as those used in this study. We built on their work by incorporating additional sediment samples from the HMA to refine their OC flux calculations, and integrating time with our own estimated contributions of OC_{terr} and OC_{mar} to establish their respective fluxes. These fluxes can then be compared with the OC fluxes from terrestrial sources (i.e., the rivers Elbe and Weser) and marine sources (i.e., on-site primary production). The sedimentation rates (SR) determined by Müller et al. (2024) have been used in this study and correlated with the corresponding OC content determined here. The regression equation (SR = (2.845 ± 0.352) × OC, $R^2 = 0.88$, $p < 0.001$; Fig. 5A) was used to extrapolate SR to other HMA sites lacking SR measurements, providing a high-resolution and reliable estimation of SR with an uncertainty of 12 % (based on the uncertainty of the correlation slope).

We estimate the recent accumulation fluxes of total sediments, terrigenous sediments (excluding carbonate and biogenic silica), OC_{mar} and OC_{terr} in the HMA using the following equations:

$$\textit{total sediment flux} = \sum_{1}^{n} \rho_{sed} \times SR \times [area] \quad (5)$$

$$\textit{terrigenous sediment flux} = \sum_{1}^{n} \rho_{sed} \times SR \times [area] \times \left(1 - f_{carbonate} - f_{BSi}\right) \quad (6)$$

$$OC_{mar}\ \textit{flux} = \sum_{1}^{n} \rho_{sed} \times SR \times [area] \times OC_{mar} \quad (7)$$

$$OC_{terr}\ \textit{flux} = \sum_{1}^{n} \rho_{sed} \times SR \times [area] \times OC_{terr} \quad (8)$$

where [area] is the area of a defined 0.01° × 0.01° grid, indicated by the number n (Fig. 5). SR is the sedimentation rate for each grid cell. The term $f_{carbonate}$ refers to the relative contribution of carbonate to each grid cell, which is remapped from the measured $f_{carbonate}$ value at each station (Table S1) using distance-weighted average. The term f_{BSi} is the relative contribution of biogenic silica to each grid cell, which averages 1.4 % in the HMA (Oehler et al., 2015). The average dry bulk density of sediment is denoted by ρ_{sed} and is estimated to be 1113 kg/m^3, based on an average sediment porosity of 0.58 (Oehler et al., 2015; Müller et al., 2024), and an average grain density of 2650 kg/m^3. The terms OC_{mar} and OC_{terr} are the content of OC_{mar} and OC_{terr} in each grid cell, respectively. Using a 0.01° × 0.01° grid, all variables were remapped to each grid cell using distance-weighted average. The accumulation fluxes of total sediment, terrigenous sediment, OC_{mar} and OC_{terr} were calculated for each grid point and summed over the grid using Eqs. (5) to (8). Fig. 5C–F depict the spatial distribution of these fluxes.

3. Results

Bulk properties, including mean grain size, carbonate content, OC content, OC loading, $(C/N)_{OC}$, and $\delta^{13}C_{OC}$ of surface sediments, showed spatial variability in the HMA and surrounding areas (Fig. 1B–F, Table S1; Wei and Holtappels, 2025). The mean grain size of all surface sediments varied from 24 to 279 μm, with low values in the HMA (54 ± 14 μm) and to the west of the HMA (66 ± 21 μm), but higher values to the east (122 ± 43 μm), the south (140 ± 64 μm) and the north (213 ± 68 μm) of the HMA (Fig. 1B). Accordingly, the SA_{cor} was generally higher in the HMA (6–30 m^2/g and mean 12 m^2/g) relative to the surrounding areas (4–13 m^2/g and mean 8 m^2/g; Fig. S1B, Table S1). The average carbonate content was also higher in the HMA (8–18 wt% and mean 13 wt%) compared to the surrounding areas (0–12 wt% and mean 5 wt%; Fig. S1A, Table S1). The OC content varied from 0.23 to 1.73 wt % in the HMA, with a mean value of 0.59 wt%, and the highest OC

content occurred in the southeast of the HMA (1.73 wt%, Fig. 1C). The OC content was also high to the west of the HMA (0.51–0.98 wt% and mean 0.67 wt%) but significantly lower in the regions surrounding the HMA, with mean values of 0.19, 0.15, and 0.10 wt% to the south, east and north of the HMA, respectively (Fig. 1C, Table S1). The OC loading (i.e., OC/SA ratio) ranged from 0.08 to 0.92 mg C/m^2, with values generally above 0.4 mg C/m^2 in the HMA and below 0.4 mg C/m^2 in the surrounding region (Fig. 1D). The $(C/N)_{OC}$ value ranged from 4.4 to 10.2 in the HMA, but could not be accurately calculated for some sandy sediments due to TN contents below the limit of quantification (Fig. 1E). The $\delta^{13}C_{OC}$ values of all surface sediments ranged from −26.4 to −22.2 ‰, increasing slightly from the Elbe River estuary (−26.4 ‰) to the HMA (−25.5 to −24.0 ‰) and surrounding sandy areas (−26.1 to −24.2 ‰), with the highest value at the northernmost sandy station (−22.2 ‰, Fig. 1F). There is no correlation between $\delta^{13}C_{OC}$ and $(C/N)_{OC}$ ratio ($R^2 = 0.21$, $p = 0.347$).

The abundance of FAs and alkanes was also spatially variable in the study area (Fig. 2A–H). The abundances of saturated FAs (C_{14} to C_{32}) in each sample showed a bimodal pattern with two pronounced peaks at C_{16} and C_{26}, respectively (Fig. 2A). The abundance of C_{16} and C_{18} FAs (i.e., C_{16+18} FAs) varied from 172 to 1243 μg/g OC (Fig. 2C), in a similar range to that of C_{26} to C_{32} FAs with even carbon number (i.e., $C_{26–32even}$ FAs, 173–1150 μg/g OC; Fig. 2E). The abundances of *i/ai*-C_{15} and *i/ai*-C_{17} FAs (i.e., $C_{15+17i/ai}$ FAs) varied between 40 and 271 μg/g OC and show a significant positive correlation with C_{16+18} FA abundances ($R^2 = 0.66$, $p < 0.001$) but an insignificant correlation with $C_{26–32even}$ FA abundances ($R^2 = 0.12$, $p = 0.054$, Fig. 2D, F). The abundance of saturated alkanes showed a unimodal pattern with a pronounced peak at C_{29} (Fig. 2B). The abundances of C_{27} to C_{35} alkanes with odd carbon numbers (i.e., $C_{27–35odd}$ alkanes) varied from 25 to 233 μg/g OC, which is considerably lower than $C_{26–32even}$ FA abundances but showed a similar spatial pattern to the $C_{26–32even}$ FA abundances ($R^2 = 0.73$, $p < 0.001$, Fig. 2E, G). The abundance of C_{26} to C_{32} alkanes with even carbon number (i.e., $C_{26–32even}$ alkanes, 7–49 μg/g OC) also showed a similar spatial distribution (Fig. 2E, G, H).

4. Discussion

4.1. OC source identification and quantification in the HMA and surrounding sandy areas

The distinct mineralogical and geochemical characteristics of

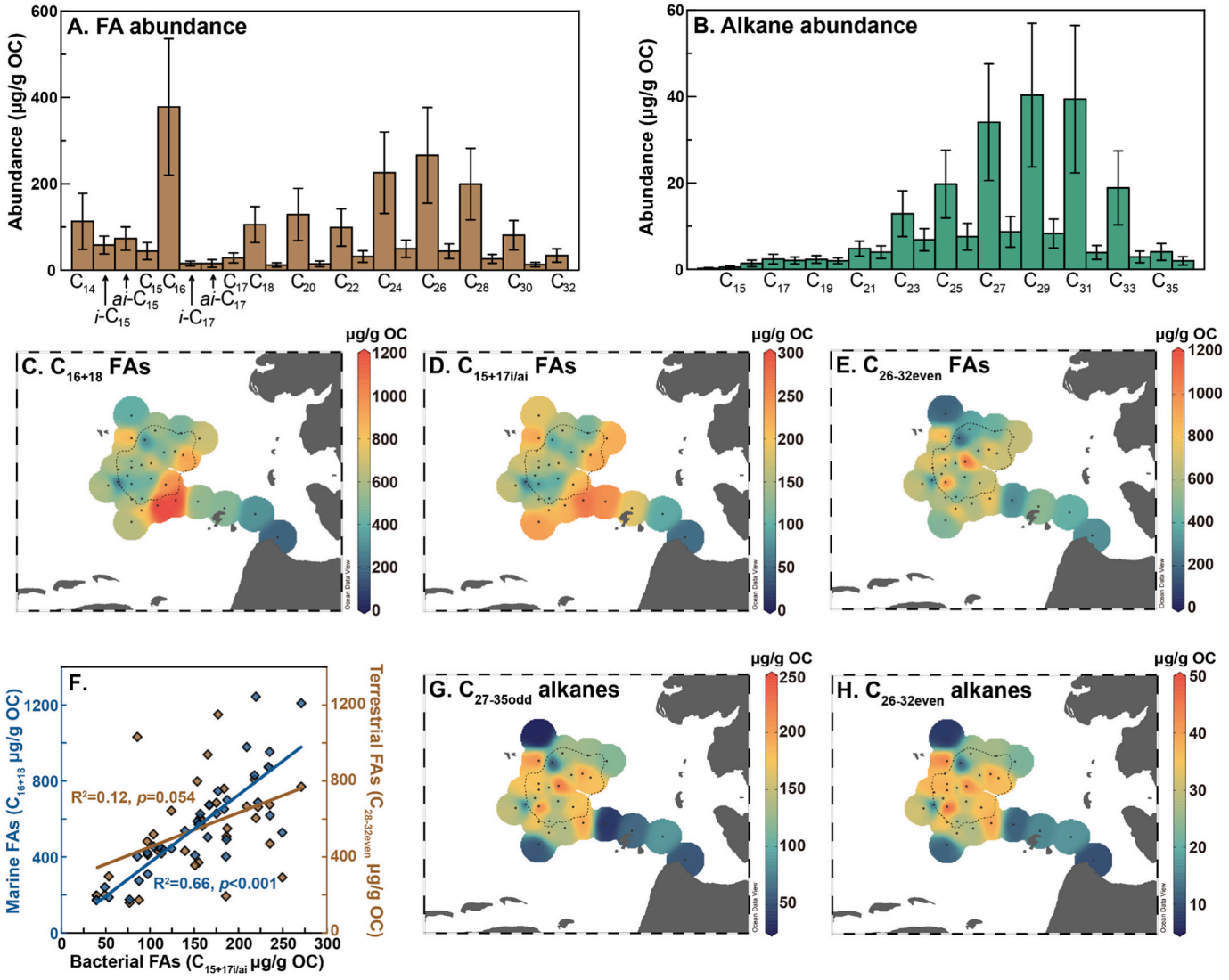

Fig. 2. Mean abundances of (A) saturated FAs (C_{14}–C_{32}) and branched FAs (*i*-C_{15}, *ai*-C_{15}, *i*-C_{17}, and *i*-C_{17}) and (B) saturated alkanes (C_{14}–C_{36}) (n = 31); Spatial abundances of (C) C_{16+18} FAs, (D) $C_{15+17i/ai}$ FAs, and (E) $C_{26–32even}$ FAs (n = 31); (F) Correlation of $C_{15+17i/ai}$ FA abundances with C_{16+18} FAs and $C_{26–32even}$ FAs abundances, respectively; Spatial abundances of (G) $C_{27–35odd}$ alkanes and (H) $C_{26–32even}$ alkanes (n = 31). In panels C–E and G–H, the dashed contour represents the extent of the HMA according to von Haugwitz et al. (1988); stations used for each plot are displayed as black dots.

sediments in the HMA and surrounding areas indicate different carbon input sources and biogeochemical processes. The HMA and the region to the west of the HMA are characterized by relatively fine-grained sediments (55 ± 15 μm on average), high contents of carbonate (13 ± 3 wt %) and OC (0.61 ± 0.32 wt%), high OC loadings (0.49 ± 0.09 m^2/g) and $(C/N)_{OC}$ ratios (7.0 ± 1.2), and ^{13}C-depleted OC (−24.7 ± 0.4 ‰) (Figs. 1B–F, S1A), indicating high carbonate and OC accumulation and substantial terrestrial input. Sediments with relatively higher OC contents (>1 wt%) in the southeastern HMA, close to the Elbe River outflow channel (Fig. 1A, D), indicate an important contribution of fine and

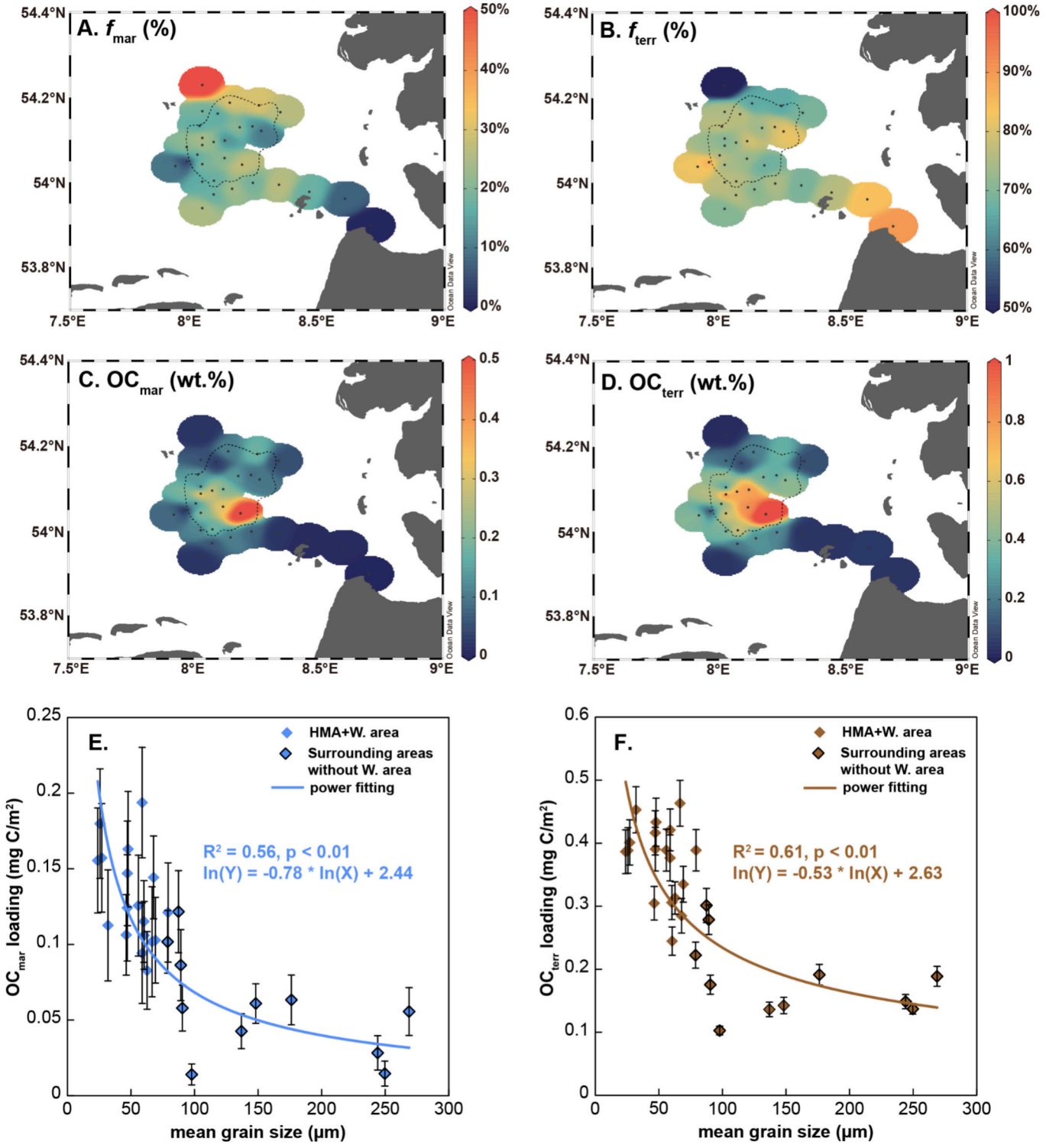

Fig. 3. Spatial distribution of relative fractions of (A) OC_{mar} (f_{mar}; $n = 31$) and (B) OC_{terr} (f_{terr}; n = 31), contents of (C) OC_{mar} (n = 31) and (D) OC_{terr} (n = 31), and correlations of (E) OC_{mar} and (F) OC_{terr} loadings with mean grain size in the HMA and surrounding areas. In panels A–D, the dashed contour represents the extent of the HMA adapted from von Haugwitz et al. (1988) and stations used for each plot are displayed as small black dots. In panels E and F, samples from the HMA and the western area adjacent to the HMA are marked without an outline, and samples from the surrounding areas, excluding the western area, are marked with a black outline.

OC_{terr}-rich sediments via riverine input, as also suggested by Müller et al. (2024). The low variability of OC loadings in the HMA (0.4–1.0 mg C/m^2, Fig. 1D) is characteristic of relatively stable organo-mineral associations and is commonly found in SPM and sediments in many river, estuarine and shelf environments (Blair and Aller, 2012 and references therein). Note that the lack of significant correlation between $\delta^{13}C_{OC}$ and $(C/N)_{OC}$ ratio ($R^2 = 0.21$, $p = 0.347$) in the study area is likely due to microbial degradation, mineralization, and sediment reworking (e.g., Lamb et al., 2006; Zonneveld et al., 2010), which can alter the original correlation typically observed between the two parameters. In contrast, the areas surrounding the HMA are characterized by coarse-grained sediments (154 ± 69 μm), low contents of carbonate (4 ± 3 wt%) and OC (0.16 ± 0.12 wt%), and low OC loadings (0.26 ± 0.11 m^2/g), reflecting low accumulation of carbonate and OC (Fig. 1B–D). The increasing $\delta^{13}C_{OC}$ values from the Elbe River estuary towards the HMA (−26.4 to −24.3 ‰, Fig. 1F) reflect continuous mixing of OC_{terr} from the Elbe River (27.2 ± 0.7 ‰; Zander et al., 2020) with autochthonous OC_{mar} into the HMA. This mixing persists despite the presence of coarse-grained sediments with low OC content along the Elbe River outflow channel as the result of strong hydrodynamics in the area. The highest $\delta^{13}C_{OC}$ value (−22.2 ‰; Fig. 1F) in the northernmost sandy station suggests a relatively higher input of OC_{mar} at this station compared to other stations. The OC loading in both of these sandy areas was generally in the range of 0.1–0.4 mg C/m^2, implying efficient net decomposition (Blair and Aller, 2012 and references therein).

Accordingly, the mixing model-based results show that the proportion of OC_{mar} in the surface sediments increased from 10 % at the site closest to the Elbe estuary to 18–34 % in the HMA (average 26 ± 5 %) and surrounding areas (average 26 ± 10 %), with another relatively low value (12 %) at the westernmost site and a remarkably high value (53 %) at the northernmost site (Fig. 3A). The proportion of OC_{terr} shows the opposite pattern, the HMA and surrounding areas are dominated by OC_{terr} (HMA: 74 ± 5 %, sandy area: 74 ± 10 %; Fig. 3B). In addition, contents of OC_{terr} and OC_{mar} at each site were calculated by multiplying the OC content by the fractional proportions of OC_{terr} and OC_{mar} to bulk OC, respectively. The OC_{terr} content averaged 0.54 ± 0.25 wt% in the HMA but only 0.11 ± 0.08 wt% in the surrounding sandy areas (Fig. 3D). The OC_{mar} content averaged 0.19 ± 0.12 wt% in the HMA and 0.04 ± 0.03 wt% in the surrounding sandy areas (Fig. 3C). Both the highest OC_{terr} and OC_{mar} contents were found in the southeastern HMA (Fig. 3C, D), indicating greater burial of OC_{terr} and OC_{mar} in this region.

4.2. Degradation and preservation of OC in the HMA and surrounding sandy areas

Two major mechanisms – selective degradation and mineral protection – have been proposed to explain OC preservation in soils and marine sediments (Hedges et al., 1997; Hemingway et al., 2019; Lalonde et al., 2012; Zonneveld et al., 2010). Mineral protection entails that OC is shielded from respiration when embedded in pore spaces and cracks of sediments inaccessible to microorganisms and enzymes (Kleber et al., 2021). In these protected environments, selective degradation depends on the OC molecule's specific degradability and the available electron acceptor (Kleber et al., 2021). In the HMA and surrounding areas, both OC_{terr} and OC_{mar} loadings are negatively correlated with mean grain size (R^2 = 0.61 and 0.56, respectively, both $p < 0.01$, Fig. 3E, F). This relationship is not straightforward to interpret, as the calculation of OC loading assumes that OC is associated with mineral surfaces, specifically the available grain surface area of the mud fraction (see Eq. (1)). If mineral protection were the sole preservation mechanism, OC loadings would be expected be similar both in fine- and coarse-grained sediments. Instead, we observed that OC_{terr} and OC_{mar} in coarser sediments appear less preserved, mostly likely due to greater oxidation driven by deeper oxygen penetration in coarser sediments (Ahmerkamp et al., 2017; Bao et al., 2016; Wei et al., 2020). This is consistent with the findings of Müller et al. (2024), who found that oxygen exposure time (or sedimentation rate) is a key factor determining the burial efficiency of OC in the fine-grained sediments of the HMA. In addition, we found a more pronounced decrease in OC_{mar} loading with grain size compared to OC_{terr} loading (−0.78 vs. −0.53; Fig. 3E, F), suggesting selective degradation of OC_{mar} over OC_{terr} with increased MGS (i.e., oxygen exposure time). Note that, we primarily focus on comparing OC_{terr} and OC_{mar} degradation across different grain sizes. While OC_{terr} loadings in marine sediments relative to the riverine OC loading would give direct insights into the extent of OC_{terr} degradation, riverine OC loading data is unavailable. Therefore, we use the OC_{terr} budget to address this question (see details in Section 4.3).

In addition to OC preservation and degradation observed at the bulk level (as discussed above), we studied the preferential degradation and preservation of OC at the molecular level, based on chemical biomarkers for specific sources (Bianchi and Canuel, 2011). In the ocean, C_{16+18} FAs are primarily derived from marine sources, although these chain lengths are ubiquitous in both eukaryotes and bacteria. In open marine settings, algal sources of C_{16+18} FAs dominate over C_{16+18} FAs derived from terrestrial vegetation and typically overwhelm bacterial contribution (e.g., Volkman et al., 1998). $C_{15+17i/ai}$ and $C_{15+17+19}$ FAs are typically from bacterial sources, and $C_{26–32even}$ FAs (leaf wax lipids) have a terrestrial biospheric OC origin (e.g., Drenzek et al., 2007; Kusch et al., 2021; Tao et al., 2016; Wei et al., 2021). The absence of substantial amounts of bacterial hopanoids, alkanes, and branched alkanes in the hydrocarbon fraction (Volkman et al., 1998) indicates that C_{16+18} FAs are mainly algae derived. The $C_{15+17i/ai}$ FA abundances are positively correlated with C_{16+18} FA abundances ($R^2 = 0.66$, $p < 0.001$, Fig. 2F), but insignificantly correlated with $C_{26–32even}$ FA abundances ($R^2 = 0.12$, $p = 0.054$, Fig. 2F). This suggests that bacteria predominantly utilize/degrade OC_{mar} rather than OC_{terr}, as supported by the predominantly marine signature of $\delta^{13}C$-DIC in the porewater of HMA sediments (Müller et al., 2024). The observed correlations reflect the selective removal of biochemically reactive OC_{mar} and retention of biochemically less reactive OC_{terr}. This does not imply that OC_{terr} will not undergo further degradation, but the OC_{terr} exported to the study area is already degraded, as OC_{terr} degradation mainly occurs in the estuary (Hou et al., 2020, 2021); in contrast, OC_{mar} is mainly degraded on site.

Despite the overall higher stability of OC_{terr} compared to OC_{mar}, biospheric and petrogenic OC_{terr} may have distinct fates in the HMA and surrounding areas. In the absence of bulk and compound-specific ^{14}C data that would allow distinguishing these OC_{terr} pools, we assess the quality of OC_{terr} using our molecular data: $C_{26–32even}$ FAs and $C_{27–35odd}$ alkanes originate from relatively fresh and less refractory biospheric OC_{terr} (Eglinton and Eglinton, 2008; Feng et al., 2013; Tao et al., 2016), whereas $C_{26–32even}$ alkanes are derived from reworked and more refractory petrogenic sources (Tao et al., 2015). In the study area, the contribution of $C_{26–32even}$ FAs and $C_{27–35odd}$ alkanes to total OC_{terr} were relatively higher in the fine-grained HMA ([$C_{26–32even}$ FAs/OC_{terr}] = 0.90 ± 0.27 mg/g, [$C_{27–35odd}$ alkanes/OC_{terr}] = 0.23 ± 0.04 mg/g) compared to the surrounding coarse-grained sediments ([$C_{26–32even}$ FAs/OC_{terr}] = 0.65 ± 0.32 mg/g, [$C_{27–35odd}$ alkanes/OC_{terr}] = 0.13 ± 0.08 mg/g) (Fig. 4A, B). In contrast, the contribution of $C_{26–32even}$ alkanes to the total OC_{terr} pool (i.e., $C_{26–32even}$ alkanes/OC_{terr}]) shows a clear increasing trend with mean grain size (Fig. 4C). These differences and trends reflect relatively higher biospheric OC_{terr} and lower petrogenic OC_{terr} contributions to the fine-grained HMA compared to the surrounding coarse sediments. Furthermore, carbon preference index (i.e., $CPI_{26–32FAs}$ and $CPI_{24–34alkanes}$) values can reflect the thermal maturity of biospheric OC_{terr}, where lower $CPI_{26–32FAs}$ values indicate a higher degradation extent (Bröder et al., 2016). Relatively higher $CPI_{26–32FAs}$ and $CPI_{24–34alkanes}$ values in the HMA than in the sandy areas also suggest a reduced degradation state of biospheric OC_{terr} in the HMA relative to the sandy areas (Fig. 4D, F). Thus, the fine-grained HMA accumulates more OC_{terr} than the surrounding sandy areas, with this OC_{terr} being less refractory due to a higher proportion of less degraded biospheric OC than in the sandy areas.

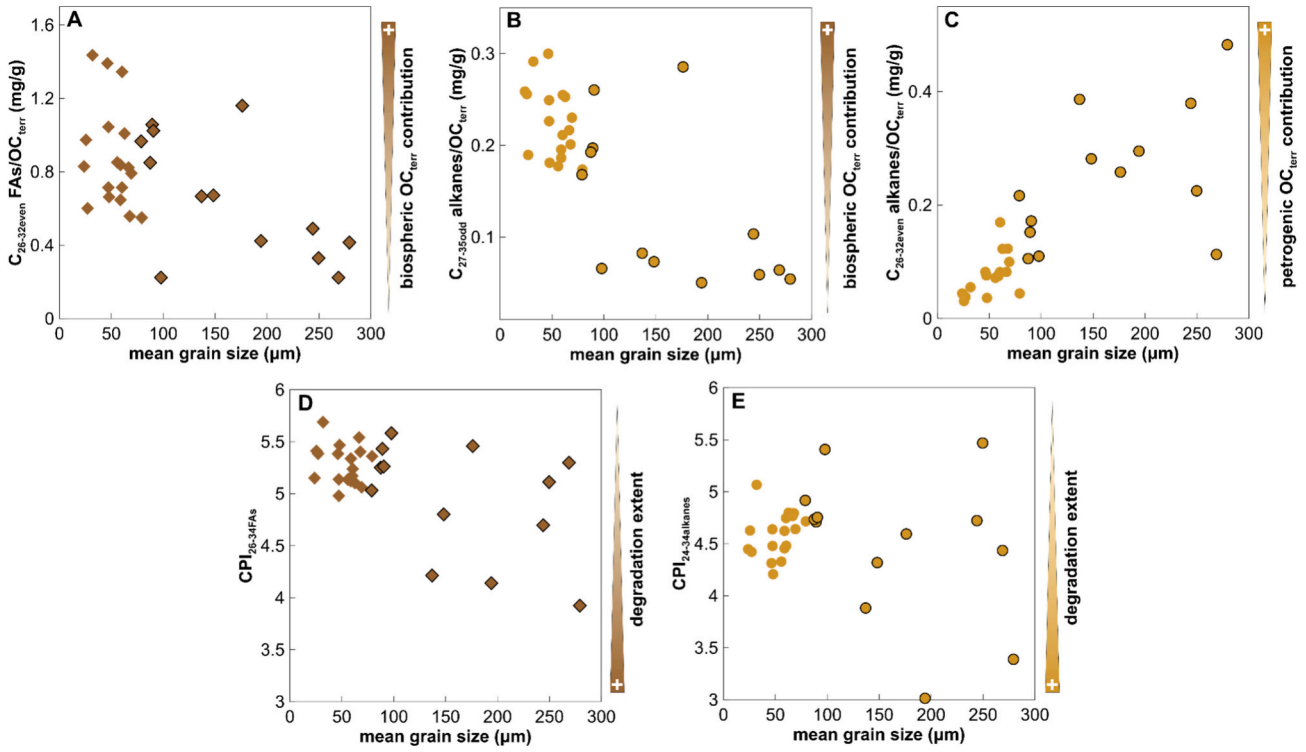

Fig. 4. Variations with mean grain size of (A) ratio of $C_{26–32even}$ FAs to total OC_{terr} content ($C_{26–32even}$ FAs/OC_{terr}), (B) ratio of $C_{27–35odd}$ alkanes to total OC_{terr} content ($C_{27–35odd}$ alkanes/OC_{terr}), and (C) the ratio of $C_{26–32\ even}$ alkanes to total OC_{terr} content ($C_{26–32even}$ alkanes/OC_{terr}), as well as carbon preference index of (D) $C_{26–32}$ FAs ($CPI_{26–32FAs}$), defined as $0.5 \times C_{26} + C_{28} + C_{30} + 0.5 \times C_{32})/(C_{27} + C_{29} + C_{31})$, and (E) $C_{24–34}$ alkanes ($CPI_{24–34alkanes}$), defined as $0.5 \times (C_{25} + C_{27} + C_{29} + C_{31} + C_{33})/(C_{24} + C_{26} + C_{28} + C_{30} + C_{32}) + 0.5 \times (C_{25} + C_{27} + C_{29} + C_{31} + C_{33})/(C_{26} + C_{28} + C_{30} + C_{32} + C_{34})$, in the HMA and surrounding areas. In the panels A–E, samples from the HMA and the western area adjacent to the HMA are marked without an outline and samples from the surrounding areas, excluding the western area, are marked with a black outline.

The distinct characteristics of OC degradation and preservation in the mud fraction of the HMA and surrounding sandy areas are probably also due to different modes of solute transport (diffusion vs. advection) in the surface sediments of each area (e.g., Oni et al., 2015; Zhou et al., 2023, 2024). Both experimental and field studies have shown that advective oxygen transport and rapid exchange between bottom water and porewater enhance decomposition of OC and removal of decomposed products in permeable sands (Ahmerkamp et al., 2020; Boudreau et al., 2001; Huettel et al., 2003, 2014; Rusch et al., 2006). Moreover, tidally driven redox-oscillations are typical for sandy sediments (Ahmerkamp et al., 2017) and give rise to frequent reduction and oxidation of iron minerals (Zhou et al., 2023), which have a large capacity to produce reactive oxygen species (van Erk et al., 2023). In contrast, fine-grained sediments in the HMA not only receive more OC, but their cohesive properties allow only diffusive transport, reducing oxygen exposure time and enhancing the preservation of OC, with larger proportion of less refractory material. Therefore, the HMA sediment properties differ from the surrounding sandy areas and more closely resembles the OC degradation and preservation properties of typical mud areas (Blair and Aller, 2012; Wei et al., 2020).

4.3. OC sequestration in the HMA and its global carbon cycle implications

The accumulation flux and burial efficiency of OC from different (i.e., marine and terrestrial) sources are crucial for determining OC sequestration and influencing the carbon cycle over varying timescales (Hilton and West, 2020). Accumulation fluxes of total sediment and terrigenous sediment in the HMA were calculated to be 1.06 ± 0.13 Tg/y and 0.92 ± 0.11 Tg/yr, respectively, with the offset of 0.14 Tg/yr representing the accumulation flux of carbonate and biogenic silica (Fig. 5C, D, Table 1). The accumulation fluxes of OC_{mar} and OC_{terr} in the HMA were estimated at $(2.54 \pm 0.68) \times 10^{-3}$ and $(6.75 \pm 0.61) \times 10^{-3}$ Tg C/yr, respectively (Fig. 5E, F, Table 1), with average relative uncertainties of 27 % and 9 % for OC_{mar} and OC_{terr} contents resulting from the isotope end-member model (Table S2). The net OC_{mar} primary production in the North Sea averages 180 g C/m^2/yr (van Leeuwen et al., 2013), based on which we calculate net OC_{mar} primary production in the HMA to be 90×10^{-3} Tg C/yr. Accordingly, the OC_{mar} accumulated in the HMA is comparable to 2.8 ± 0.8 % of the OC_{mar} produced in the HMA via primary production, nearly twice the global average (<1.3 %; Burdige, 2005). The estimated terrigenous sediment flux in the HMA (0.92 ± 0.11 Tg/yr) accounts for 79 % of the total sediment flux of 1.17 Tg/yr from the Elbe (0.84 Tg/yr) and Weser (0.33 Tg/yr) rivers (Milliman and Farnsworth, 2011), with the remainder (~0.25 Tg/yr) being transported to other areas (such as the Norwegian Trough; Diesing et al., 2021). The terrigenous sediments and OC from other sources (such as the Maas, Rhine and Scheldt rivers) likely contribute to the HMA via the coastal currents, but no data are available to quantify the respective net fluxes to the HMA. Regardless, the HMA seems to be an important trap for terrigenous sediments from nearby rivers. Using the average OC content of ~2.0 wt% in exported SPM from the Elbe River (Zander et al., 2020) and ~ 2.45 wt% from the Weser River (Selje and Simon, 2003), the export of OC_{terr} from the rivers Elbe and Weser to the North Sea is estimated to be 24.89×10^{-3} Tg C/yr. Hence, the estimated OC_{terr} burial flux in the HMA is approximately 34.3 ± 3.1 % of the OC_{terr} export flux from the Elbe and Weser rivers, which is also twice the global average OC_{terr} burial efficiency in continental margin sediments (17 ± 4 %; Burdige, 2005). In addition, Müller et al. (2024) estimated that about 46 % of the total OC_{mar} and OC_{terr} is degraded upon deposition in surface sediments (up to 2 cm). Based on this determined mineralization rate of OC, we can estimate that a total flux of $(17.20 \pm 1.20) \times 10^{-3}$ Tg C/yr of OC_{mar} and OC_{terr} may reach the seafloor in the HMA (Table 1). Of the

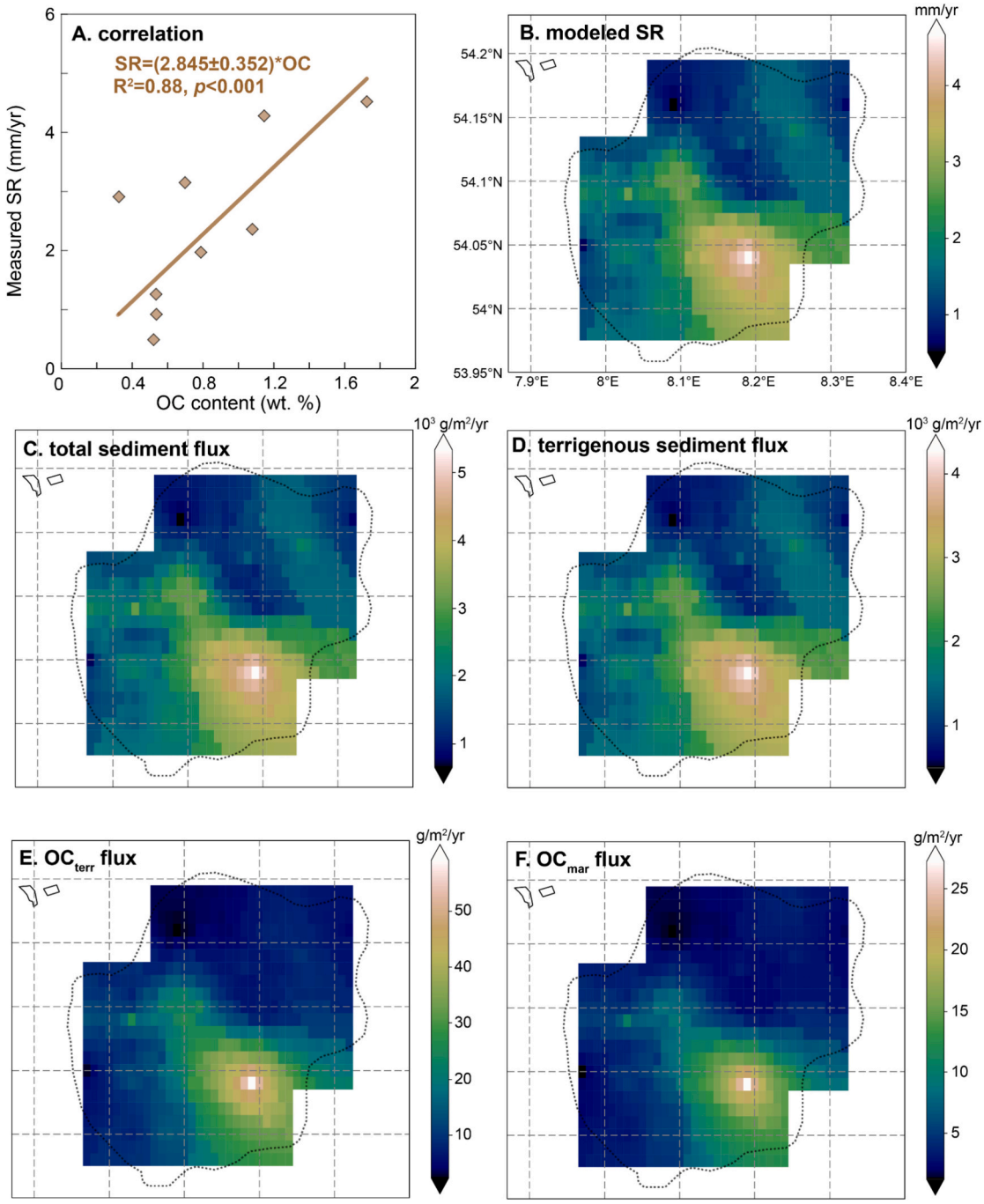

Fig. 5. (A) The correlation between measured sedimentation rate (SR) and OC content, and the spatial distribution of modeled (B) SR, (C) total sediment flux, (D) terrigenous sediment flux, (E) OC_{terr} flux and (F) OC_{mar} flux in the HMA. In panels B–F, the dashed contour represents the extent of the HMA adapted from von Haugwitz et al. (1988).

total OC_{mar} and OC_{terr} input to the HMA (109.66×10^{-3} Tg C/yr), 84 ± 2 % undergo degradation in the water column before reaching the seafloor, 7 ± 1 % continue to be degraded upon deposition, and the remaining 8 ± 1 % are ultimately buried (Table 1).

Our findings suggest that, within the uncertainties imposed by missing lateral fluxes (as outlined above), the HMA functions as a highly efficient sink for both OC_{mar} and OC_{terr}, with burial efficiencies approximately double the global average. This emphasizes the importance of accurately assessing carbon sequestration capacity and efficiency in other similar environments and their broader role in the global carbon cycle. Additionally, given that around 75 % of the sequestered OC is of terrestrial origin, any change in river sediment discharge due to changes in precipitation, land use, or river hydrodynamics (e.g., river deepening for shipping purposes) are expected to alter the accumulation fluxes of OC in the HMA. Intense bottom trawling in the northwestern HMA could further reduce OC sequestration by about 30 % by resuspending sediments into the water column, which increases oxygen exposure and thereby enhances OC remineralization (Müller et al., 2024). This suggests that the efficiency of the HMA as an OC sink would likely be higher in the absence of bottom trawling. These findings highlight the necessity of accurately interpreting historical sedimentary records in the HMA and other similar environments. Such accurate interpretation is essential for assessing the impact of management measures, such as the protection of accumulating sediments from

Table 1
A budget of sediments and OC accumulation in the HMA (details in the calculation of the fluxes are described in Section 4.3).

Sediment accumulation flux in the HMA	Total (Tg/yr)	Terrestrial (Tg/yr)	Carbonate & BSi (Tg/yr)
	1.06 ± 0.13[a]	0.92 ± 0.11[a]	0.14[a]
Terrestrial sediment flux from Weser & Elbe	Total input (Tg/yr)	Burial in HMA (Tg/yr)	Export to other areas (Tg/yr)
	1.17[b]	0.92 ± 0.11[a]	0.25
OC Flux in the HMA	Total OC (10^{-3} Tg C/yr)	OC_{mar} (10^{-3} Tg C/yr)	OC_{terr} (10^{-3} Tg C/yr)
Input	109.66	90[c]	19.66[d]
Degradation in seawater	92.46		
Export to sediments	17.20 ± 1.20		
Degradation in sediments	7.91 ± 0.78[f]		
Burial in sediments	9.29 ± 0.91	2.54 ± 0.68[e]	6.75 ± 0.61[e]
Burial efficiency	8.5 ± 0.8 %[e]	2.8 ± 0.8 %[e]	34.3 ± 3.1 %[e]

[a] Calculated based on Oehler et al. (2015), Müller et al. (2024) and on this study.
[b] Calculated based on Milliman and Farnsworth (2011).
[c] Calculated based on van Leeuwen et al. (2013).
[d] Calculated based on Selje and Simon (2003) and Zander et al. (2020).
[e] Calculated based on this study.
[f] Calculated based on Müller et al. (2024).

bottom-impacting activities. Overall, this new information provides a baseline for a better understanding of OC degradation and sequestration in the North Sea.

Small-size depocenters surrounded by sandy sediments, such as the HMA, have received less attention compared to larger and more prominent depocenters, such as extensive mud belts formed by larger rivers along coastal regions. Comprehensive data on the distribution, proportion, and contribution of these small-size depocenters to global carbon burial remain limited (see e.g., Hanebuth et al., 2015). However, a closer examination of sandy continental shelves worldwide reveals several similar hotspots (Table 2). These examples exhibit a wide range in area, from 97 to 16,254 km^2, SR ranging from 0.1 to 2.15 cm/yr and OC burial rates between 10 and 169 g m^{-2} yr^{-2} (Table 2). These findings highlight the broader implications of small-depocenters on sandy shelves as potential hotspots for OC burial. Moreover, our study emphasizes the disproportionately high carbon burial efficiency in the HMA, similar to the Southwest Cheju Mud Patch, which exhibits a high burial efficiency of 37 % for OC_{terr} and 18 % for OC_{mar} (Shi et al., 2024). These results offer evidence that small depocenters on sandy shelves can act as OC hotspots and provide a foundation for future research aimed at better quantifying their global distribution and contributions to OC burial. We encourage future studies to systematically evaluate the global distribution and significance of these systems, both in contemporary contexts and historically. Such studies will shed light on an often-overlooked aspect of OC cycling in marine sediments and contribute to a broader understanding of OC dynamics at the interface of sandy and finer-grained sedimentary environments.

5. Summary and conclusion

Spatial variations in mean grain size, OC content, OC loading, and $\delta^{13}C_{OC}$ of surface sediments in the HMA and surrounding sandy areas reflect different OC sources and specific degradation and preservation processes. In the surface sediments of the HMA and surrounding sandy areas, OC is predominantly derived from terrestrial sources (74 %), with the remaining ~26 % originating from marine sources. OC_{terr} and OC_{mar} contents were significantly higher in the sediments of the HMA (0.54 ± 0.25 wt% and 0.19 ± 0.12 wt%, respectively) compared to the surrounding areas (0.11 ± 0.08 wt% and 0.04 ± 0.03 wt%, respectively). Both OC_{terr} and OC_{mar} loadings (OC/SA) were negatively correlated with mean grain size, reflecting decreased degradation in fine-grained deposits. Molecular-level analyses further revealed relatively higher biospheric OC_{terr} (with a lower degradation state) and lower petrogenic OC_{terr} contributions in the fine-grained HMA sediments relative to the surrounding sandy sediments. These differences may be attributed to distinctions in porewater transport mechanisms (diffusive versus advective) and associated oxygen penetration depth, which determine the oxygen exposure time of the accumulated OC and ultimately affect its preservation in the sediments. Finally, we estimated the accumulation fluxes of $(6.75 \pm 0.61) \times 10^{-3}$ and $(2.54 \pm 0.68) \times 10^{-3}$ Tg C/yr for OC_{terr} and OC_{mar}, respectively, in the HMA, equivalent to 34.3 % of the OC_{terr} export from the Elbe and Weser rivers and 2.8 % of the net OC_{mar} production, respectively. Together, these estimates are twice the global average in the shelf area, indicating that the HMA resemble the OC degradation and preservation properties of typical mud areas and is an even more efficient sink for both OC_{mar} and OC_{terr}.

Table 2
Characterization of representative examples of small-size depocenters globally (M. P. = mud patch).

Region	Name	Water depth (m)	Area (km^2)	SR (cm/yr)	OC burial rate (g m^{-2} yr^{-1})	References
I. North Sea	HMA	15–35	500	0.05–0.45	19	This study
II. Bay of Biscay	Basque M. P.	50–200	700	0.13–0.50	n.a.	Dubosq et al., 2021; Jouanneau et al., 2008
	Gironde M. P.	30–75	600	0.29–0.47	28–45	
III. Iberian Margin	Muros M. P.	100–120	400	n.a.	n.a.	Abrantes et al., 2005; Dias et al., 2002; Lantzsch et al., 2009; Lebreiro et al., 2006
	Galiza M. P.	110–120	600	0.1–0.23	n.a.	
	Douro M. P.	65–130	546	0.17–0.4	n.a.	
	Tagus M. P.	88–96	340	0.51	169	
	Muros Ria	33–38	97	0.42–0.72	n.a.	
IV. Atlantic Bight	New England M. P.	50–150	13,470	0.21–0.39	16–30	Chaytor et al., 2022; Boehm, 1984; Boesch and Rabalais, 1987
	Mid and South Atlantic Bight	Not estimated but found in depression and cape-associated "shadows"				
V. West America Margin	Eel margin	10–50	363	1.3–3.3	n.a.	Crockett and Nittrouer, 2004
VI. Bering Sea	North Norton Sound	10–30	~1000	n.a.	n.a.	Drake et al., 1980
VII. China marginal sea	Southwest Cheju Island M. P.	50–100	16,254	0.2–2.15	33	Huh et al., 1990; Kao et al., 2008; Shi et al., 2024; Tao et al., 2023
	Taiwan Strait M. P.	10–30	~3000	0.50–0.80	10–40	
VIII. Australian continental shelf	Shoalhaven M. P.	75–110	285	n.a.	n.a.	Abballe and Chivas, 2017

CRediT authorship contribution statement

Bingbing Wei: Conceptualization, Formal analysis, Investigation, Writing – original draft. **Daniel Müller:** Investigation, Writing – review & editing. **Stephanie Kusch:** Conceptualization, Formal analysis, Writing – review & editing. **Lu Niu:** Formal analysis. **Jens Hefter:** Investigation, Writing – review & editing. **Lasse Sander:** Investigation, Writing – review & editing. **Ulrike Hanz:** Investigation, Writing – review & editing. **Gesine Mollenhauer:** Writing – review & editing. **Guodong Jia:** Investigation, Writing – review & editing. **Sabine Kasten:** Writing – review & editing, Funding acquisition. **Moritz Holtappels:** Conceptualization, Writing – review & editing, Supervision, Funding acquisition.

Declaration of competing interest

The authors declare that they have no known competing financial interests or personal relationships that could have appeared to influence the work reported in this paper.

Acknowledgements

We gratefully thank the captain and the crew of R/V Heincke for their support during the cruise HE595 (grant number: HE - 595). Moreover, we thank Valéa Schumacher for TOC and TN measurements, and Dr. Lingdi Chen for assistance with stable carbon isotope measurements. Funding was provided by the German Federal Ministry of Education and Research (BMBF) MARE:N project “Anthropogenic impacts on particulate organic carbon cycling in the North Sea (APOC)” (No: 03F0874A), the German Research Foundation (DFG) Cluster of Excellence “The Ocean Floor – Earth’s Uncharted Interface” (No: EXC-2077-3907411603) and the Helmholtz Association (Alfred Wegener Institute Helmholtz Centre for Polar and Marine Research) in the framework of the Helmholtz Research Program “Changing Earth – Sustaining our Future” in PoF IV.

Appendix A. Supplementary data

Supplementary data to this article can be found online at https://doi.org/10.1016/j.chemgeo.2025.122712.

Data availability

Data are available in the PANGAEA data repository (Wei and Holtappels, 2025) at https://doi.org/10.1594/PANGAEA.971520

References

Abballe, P.A., Chivas, A.R., 2017. Organic matter sources, transport, degradation and preservation on a narrow rifted continental margin: Shoalhaven, Southeast Australia. Org. Geochem. 112, 75–92.
Abrantes, F., Lebreiro, S., Rodrigues, T., Gil, I., Bartels-Jónsdóttir, H., Oliveira, P., Kissel, C., Grimalt, J.O., 2005. Shallow-marine sediment cores record climate variability and earthquake activity off Lisbon (Portugal) for the last 2000 years. Quat. Sci. Rev. 24, 2477–2494.
Ahmerkamp, S., Winter, C., Krämer, K., de Beer, D., Janssen, F., Friedrich, J., Kuypers, M. M.M., Holtappels, M., 2017. Regulation of benthic oxygen fluxes in permeable sediments of the coastal ocean. Limnol. Oceanogr. 62, 1935–1954.
Ahmerkamp, S., Marchant, H.K., Peng, C., Probandt, D., Littmann, S., Kuypers, M.M.M., Holtappels, M., 2020. The effect of sediment grain properties and porewater flow on microbial abundance and respiration in permeable sediments. Sci. Rep. 10, 1–12.
Andersson, A., Deng, J., Du, K., Zheng, M., Yan, C., Sköld, M., Gustafsson, Ö., 2015. Regionally-varying combustion sources of the january 2013 severe haze events over eastern China. Environ. Sci. Technol. 49, 2038–2043.
Bao, R., McIntyre, C., Zhao, M., Zhu, C., Kao, S.J., Eglinton, T.I., 2016. Widespread dispersal and aging of organic carbon in shallow marginal seas. Geology 44, 791–794.
Bauer, J.E., Cai, W.J., Raymond, P.A., Bianchi, T.S., Hopkinson, C.S., Regnier, P.A.G., 2013. The changing carbon cycle of the coastal ocean. Nature 504, 61–70.
Bianchi, T.S., Canuel, E.A., 2011. Chemical Biomarker in Aquatic Ecosystems. Princeton unversity press, Princeton and Oxford.
Bianchi, T.S., Cui, X., Blair, N.E., Burdige, D.J., Eglinton, T.I., Galy, V., 2018. Centers of organic carbon burial and oxidation at the land-ocean interface. Org. Geochem. 115, 138–155.
Blair, N.E., Aller, R.C., 2012. The fate of terrestrial organic carbon in the marine environment. Annu. Rev. Mar. Sci. 4, 401–423.
Blott, S.J., Pye, K., 2001. Gradistat: a grain size distribution and statistics package for the analysis of unconcolidated sediments. Earth Surf. Process. Landf. 26, 1237–1248.
Bockelmann, F.D., Puls, W., Kleeberg, U., Müller, D., Emeis, K.C., 2018. Mapping mud content and median grain-size of North Sea sediments – a geostatistical approach. Mar. Geol. 397, 60–71.
Boehm, P.D., 1984. Aspects of the saturated hydrocarbon geochemistry of recent sediments in the Georges Bank region. Org. Geochem. 7, 11–23.
Boesch, D.F., Rabalais, N.N., 1987. Long-Term Environmental Effects of Offshore Oil and Gas Development. Taylor & Francis.
Boudreau, B.P., Huettel, M., Forster, S., Jahnke, R.A., McLachlan, A., Middelburg, J.J., Nielsen, P., Sansone, F., Taghon, G., Van Raaphorst, W., Webster, I., Weslawski, J.M., Wiberg, P., Sundby, B., 2001. Permeable marine sediments: overturning an old paradigm. Eos (Washington, DC) 82, 133–136.
Bröder, L., Tesi, T., Salvadó, J.A., Semiletov, I.P., Dudarev, O.V., Gustafsson, O., 2016. Fate of terrigenous organic matter across the Laptev Sea from the mouth of the Lena River to the deep sea of the Arctic interior. Biogeosciences 13, 5003–5019.
Burdige, D.J., 2005. Burial of terrestrial organic matter in marine sediments: a re-assessment. Glob. Biogeochem. Cycles 19, 1–7.
Chaytor, J.D., Ballard, M.S., Buczkowski, B.J., Goff, J.A., Lee, K.M., Reed, A.H., Boggess, A.A., 2022. Measurements of geologic characteristics and geophysical properties of sediments from the New England Mud Patch. IEEE J. Ocean. Eng. 47, 503–530.
Crockett, J.S., Nittrouer, C.A., 2004. The sandy inner shelf as a repository for muddy sediment: an example from Northern California. Cont. Shelf Res. 24, 55–73.
de Haas, H., Van Weering, T.C.E., De Stigter, H., 2002. Organic carbon in shelf seas: sinks or sources, processes and products. Cont. Shelf Res. 22, 691–717.
Dias, J.M.A., Jouanneau, J.M., Gonzalez, R., Araújo, M.F., Drago, T., Garcia, C., Oliveira, A., Rodrigues, A., Vitorino, J., Weber, O., 2002. Present day sedimentary processes on the northern Iberian shelf. Prog. Oceanogr. 52, 249–259.
Diesing, M., Thorsnes, T., Rún Bjarnadóttir, L., 2021. Organic carbon densities and accumulation rates in surface sediments of the North Sea and Skagerrak. Biogeosciences 18, 2139–2160.
Drake, D.E., Cacchione, D.A., Muench, R.D., Nelson, C.H., 1980. Sediment transport in Norton Sound, Alaska. Mar. Geol. 36, 97–126.
Drenzek, N.J., Montluçon, D.B., Yunker, M.B., Macdonald, R.W., Eglinton, T.I., 2007. Constraints on the origin of sedimentary organic carbon in the Beaufort Sea from coupled molecular ^{13}C and ^{14}C measurements. Mar. Chem. 103, 146–162.
Dubosq, N., Schmidt, S., Walsh, J.P., Grémare, A., Gillet, H., Lebleu, P., Poirier, D., Perello, M.C., Lamarque, B., Deflandre, B., 2021. A first assessment of organic carbon burial in the West Gironde Mud Patch (Bay of Biscay). Cont. Shelf Res. 221.
Eglinton, T.I., Eglinton, G., 2008. Molecular proxies for paleoclimatology. Earth Planet. Sci. Lett. 275, 1–16.
Emery, K.O., 1968. Relict sediments on continental shelves of world. Am. Assoc. Pet. Geol. Bull. 52, 445–464.
Feng, X., Benitez-Nelson, B.C., Montluçon, D.B., Prahl, F.G., McNichol, A.P., Xu, L., Repeta, D.J., Eglinton, T.I., 2013. ^{14}C and ^{13}C characteristics of higher plant biomarkers in Washington margin surface sediments. Geochim. Cosmochim. Acta 105, 14–30.
Galy, V., Peucker-Ehrenbrink, B., Eglinton, T., 2015. Global carbon export from the terrestrial biosphere controlled by erosion. Nature 521, 204–207.
Hanebuth, T.J.J., Lantzsch, H., Nizou, J., 2015. Mud depocenters on continental shelves—appearance, initiation times, and growth dynamics. Geo-Mar. Lett. 35, 487–503.
Hartnett, H.E., Keil, R.G., Hedges, J.I., Devol, A.H., 1998. Influenceof oxygen exposure time on organic carbon preservation in continental marginsediments. Nature 391, 2–4.
Hebbeln, D., Scheurle, C., Lamy, F., 2003. Depositional history of the Helgoland mud area, German Bight, North Sea. Geo-Mar. Lett. 23, 81–90.
Hedges, J.I., Keil, R.G., Benner, R., 1997. What happens to terrestrial organic matter in the ocean? Org. Geochem. 27, 195–212.
Hemingway, J.D., Rothman, D.H., Grant, K.E., Rosengard, S.Z., Eglinton, T.I., Derry, L.A., Galy, V.V., 2019. Mineral protection regulates long-term global preservation of natural organic carbon. Nature 570, 228–231.
Hilton, R.G., West, A.J., 2020. Mountains, erosion and the carbon cycle. Nat. Rev. Earth Environ. 1.
Hou, P., Yu, M., Zhao, M., Montluçon, D.B., Su, C., Eglinton, T.I., 2020. Terrestrial biomolecular burial efficiencies on continental margins. J. Geophys. Res. Biogeosci. 125.
Hou, P., Eglinton, T.I., Yu, M., Montluçon, D.B., Haghipour, N., Zhang, H., Jin, G., Zhao, M., 2021. Degradation and aging of terrestrial organic carbon within estuaries: biogeochemical and environmental implications. Environ. Sci. Technol. 55, 10852–10861.
Huettel, M., Røy, H., Precht, E., Ehrenhauss, S., 2003. Hydrodynamical impact on biogeochemical processes in aquatic sediments. Hydrobiologia 494, 231–236.
Huettel, M., Berg, P., Kostka, J.E., 2014. Benthic exchange and biogeochemical cycling in permeable sediments. Annu. Rev. Mar. Sci. 6, 23–51.
Huh, C.A., Small, L.F., Niemnil, S., Finney, B.P., Hickey, B.M., Kachel, N.B., Gorsline, D. S., Williams, P.M., 1990. Sedimentation dynamics in the Santa Monica-San Pedro Basin off Los Angeles: radiochemical, sediment trap and transmissometer studies. Cont. Shelf Res. 10, 137–164.

Jouanneau, J.M., Weber, O., Champilou, N., Cirac, P., Muxika, I., Borja, A., Pascual, A., Rodríguez-Lázaro, J., Donard, O., 2008. Recent sedimentary study of the shelf of the Basque country. J. Mar. Syst. 72, 397–406.
Kao, S.J., Jan, S., Hsu, S.C., Lee, T.Y., Dai, M., 2008. Sediment budget in the Taiwan Strait with high fluvial sediment inputs from mountainous rivers: new observations and synthesis. Terr. Atmos. Ocean. Sci. 19, 525–546.
Kleber, M., Bourg, I.C., Coward, E.K., Hansel, C.M., Myneni, S.C.B., Nunan, N., 2021. Dynamic interactions at the mineral–organic matter interface. Nat. Rev. Earth Environ. 2, 402–421.
Krause, G., Budeus, G., Gerdes, D., Schaumann, K., Hesse, K., 1986. Frontal systems in the german bight and their physical and biological effects. Elsevier Oceanogr. Ser. 42, 119–140.
Kusch, S., Mollenhauer, G., Willmes, C., Hefter, J., Eglinton, T.I., 2021. Controls on the age of plant waxes in marine sediments – a global synthesis. Org. Geochem. 157, 104259.
Lalonde, K., Mucci, A., Ouellet, A., Gélinas, Y., 2012. Preservation of organic matter in sediments promoted by iron. Nature 483, 198–200.
Lamb, A.L., Wilson, G.P., Leng, M.J., 2006. A review of coastal palaeoclimate and relative sea-level reconstructions using $\delta^{13}C$ and C/N ratios in organic material. Earth-Sci. Rev. 75, 29–57.
Lantzsch, H., Hanebuth, T.J.J., Bender, V.B., 2009. Holocene evolution of mud depocentres on a high-energy, low-accumulation shelf (NW Iberia). Quat. Res. 72, 325–336.
Lebreiro, S.M., Francés, G., Abrantes, F.F.G., Diz, P., Bartels-Jónsdóttir, H.B., Stroynowski, Z.N., Gil, I.M., Pena, L.D., Rodrigues, T., Jones, P.D., Nombela, M.A., Alejo, I., Briffa, K.R., Harris, I., Grimalt, J.O., 2006. Climate change and coastal hydrographic response along the Atlantic Iberian margin (Tagus Prodelta and Muros Ría) during the last two millennia. Holocene 16, 1003–1015.
Mayer, L.M., Rossi, P.M., 1982. Specific surface areas in coastal sediments: relationships with other textural factors. Mar. Geol. 45, 241–252.
Megens, L., Van Der Plicht, J., De Leeuw, J.W., 2001. C and ^{14}C concentrations in particulate organic matter from the southern North Sea. Geochim. Cosmochim. Acta 65, 2899–2911.
Middelburg, J.J., Nieuwenhuize, J., 1998. Carbon and nitrogen stable isotopes in suspended matter and sediments from the Schelde Estuary. Mar. Chem. 60, 217–225.
Milliman, J.D., Farnsworth, L.K., 2011. River discharge to the coastal ocean: a global synthesis. Cambridge University Press.
Mollenhauer, G., Eglinton, T.I., 2007. Diagenetic and sedimentological controls on the composition of organic matter preserved in California Borderland Basin sediments. Limnol. Oceanogr. 52, 558–576.
Müller, D., Liu, B., Geibert, W., Holtappels, M., Sander, L., Miramontes, E., Taubner, H., Henkel, H., Hinrichs, K., Bethke, D., Dohrmann, M., Kasten, S., 2024. Depositional controls and budget of organic carbon burial in fine-grained sediments of the North Sea – the Helgoland Mud Area as a test field. EGUsphere 2024. https://doi.org/10.5194/egusphere-2024-1632 [preprint].
Oehler, T., Schlüter, M., Schückel, U., 2015. Seasonal dynamics of the biogenic silica cycle in surface sediments of the Helgoland Mud Area (southern North Sea). Cont. Shelf Res. 107, 103–114.
Oni, O.E., Schmidt, F., Miyatake, T., Kasten, S., Witt, M., Hinrichs, K.U., Friedrich, M.W., 2015. Microbial communities and organic matter composition in surface and subsurface sediments of the Helgoland mud area, North Sea. Front. Microbiol. 6, 1–16.
Porz, L., Zhang, W., Hanebuth, T.J.J., Schrum, C., 2021. Physical processes controlling mud depocenter development on continental shelves – geological, oceanographic, and modeling concepts. Mar. Geol. 432.
Rusch, A., Huettel, M., Wild, C., Reimers, C.E., 2006. Benthic oxygen consumption and organic matter turnover in organic-poor, permeable shelf sands. Aquat. Geochem. 12, 1–19.
Schubert, C.J., Calvert, S.E., 2001. Nitrogen and carbon isotopic composition of marine and terrestrial organic matter in Arctic Ocean sediments: implications for nutrient utilization and organic matter composition. Deep. Res. I Oceanogr. Res. Pap. 48, 789–810.
Schlitzer, R., 2019. Ocean Data View.
Selje, N., Simon, M., 2003. Composition and dynamics of particle-associated and free-living bacterial communities in the Weser estuary, Germany. Aquat. Microb. Ecol. 30, 221–237.
Shi, X., Wu, B., Qiao, S., Yao, Z., Hu, L., Bai, Y., Hu, S., Sheng, J., Liu, Y., Liu, S., Wang, K., Zou, J., 2024. Distribution, burial fluxes and carbon sink effect of sedimentary organic carbon in the eastern China seas. Sci. China Earth Sci. 67.
Sun, X., Hu, L., Fan, D., Wang, H., Yang, Z., Guo, Z., 2024. Sediment resuspension accelerates the recycling of terrestrial organic carbon at a large river-coastal ocean interface. Glob. Biogeochem. Cycles 38 (7), 1–25.
Tao, S., Eglinton, T.I., Montluçon, D.B., McIntyre, C., Zhao, M., 2015. Pre-aged soil organic carbon as a major component of the Yellow River suspended load: regional significance and global relevance. Earth Planet. Sci. Lett. 414, 77–86.
Tao, S., Eglinton, T.I., Montluçon, D.B., McIntyre, C., Zhao, M., 2016. Diverse origins and pre-depositional histories of organic matter in contemporary Chinese marginal sea sediments. Geochim. Cosmochim. Acta 191, 70–88.
Tao, S., Wang, A., Liu, J.T., Ye, X., Blattmann, T.M., Ran, C., Liu, Z., Wang, L., Yin, X., Zhang, H., Li, L., Ning, X., Hung, C.C., Haghipour, N., 2023. Characteristics of sedimentary organic carbon burial in the shallow conduit portion of source-to-sink sedimentary systems in marginal seas. Geochim. Cosmochim. Acta 353, 92–111.
van Beusekom, J.E.E., Brockmann, U.H., Hesse, K.-J., Hickel, W., Poremba, K., Tillmann, U., 1999. The importance of sediments in the transformation and turnover of nutrients and organic matter in the Wadden Sea and German Bight. Dtsch. Hydrogr. Zeitschrift 51, 245–266.
van Erk, M.R., Bourceau, O.M., Moncada, C., Basu, S., Hansel, C.M., De Beer, D., 2023. Reactive oxygen species affect the potential for mineralization processes in permeable intertidal flats. Nat. Commun. 1–10.
van Leeuwen, S.M., van der Molen, J., Ruardij, P., Fernand, L., Jickells, T., 2013. Modelling the contribution of deep chlorophyll maxima to annual primary production in the North Sea. Biogeochemistry 113, 137–152.
Volkman, J.K., Barrett, S.M., Blackburn, S.I., Mansour, M.P., Sikes, E.L., Gelin, F., 1998. Microalgal biomarkers: a review of recent research developments. Org. Geochem. 29, 1163–1179.
von Haugwitz, W., Wong, H.K., Salge, U., 1988. The mud area southeast of Helgoland: a reflection seismic study. Mitt. Geol. Palaeont. Inst. Univ. Hamburg 65, 409–422.
Wei, B., Holtappels, M., 2025. Geochemical Properties in Surface Sediments of the Helgoland Mud Area and Surrounding Sandy Areas Taken during HEINCKE Cruise HE595 in the North Sea [dataset bundled publication]. PANGAEA.
Wei, B., Mollenhauer, G., Hefter, J., Grotheer, H., Jia, G., 2020. Dispersal and aging of terrigenous organic matter in the Pearl River Estuary and the northern South China Sea Shelf. Geochim. Cosmochim. Acta 282, 324–339.
Wei, B., Mollenhauer, G., Hefter, J., Kusch, S., Grotheer, H., Schefuß, E., Jia, G., 2021. The nature, timescale, and efficiency of riverine export of terrestrial organic carbon in the (sub)tropics: insights at the molecular level from the Pearl River and adjacent coastal sea. Earth Planet. Sci. Lett. 565.
Yu, M., Eglinton, T.I., Hou, P., Haghipour, N., Zhang, H., Wang, Z., Zhao, M., 2024. Apparent aging and rejuvenation of terrestrial organic carbon along the river-estuary-coastal ocean continuum. Geophys. Res. Lett. 51 (8), 1–11.
Zander, F., Heimovaara, T., Gebert, J., 2020. Spatial variability of organic matter degradability in tidal Elbe sediments. J. Soils Sediments 20, 2573–2587.
Zhou, Z., Henkel, S., Kasten, S., Holtappels, M., 2023. The iron “redox battery” in sandy sediments: its impact on organic matter remineralization and phosphorus cycling. Sci. Total Environ. 865, 161–168.
Zhou, Z., Waska, H., Henkel, S., Dittmar, T., Kasten, S., Holtappels, M., 2024. Iron promotes the retention of terrigenous dissolved organic matter in subtidal permeable sediments. Environ. Sci. Technol. 58, 6204–6214.
Zonneveld, K.A.F., Versteegh, G.J.M., Kasten, S., Eglinton, T.I., Emeis, K.C., Huguet, C., Koch, B.P., De Lange, G.J., De Leeuw, J.W., Middelburg, J.J., Mollenhauer, G., Prahl, F.G., Rethemeyer, J., Wakeham, S.G., 2010. Selective preservation of organic matter in marine environments; processes and impact on the sedimentary record. Biogeosciences 7, 483–511.